Absorption and wavelength modulation spectroscopy of NO$_2$ using a tunable, external cavity continuous wave quantum cascade laser

Andreas Karpf* and Gottipaty N. Rao

Department of Physics, Adelphi University, Garden City, New York 11530, USA

*Corresponding author: karpf@adelphi.edu

The absorption spectra and wavelength modulation spectroscopy (WMS) of NO$_2$ using a tunable, external cavity CW quantum cascade laser operating at room temperature in the region of 1625 to 1645 cm^{-1} are reported. The external cavity quantum cascade laser enabled us to record continuous absorption spectra of low concentrations of NO$_2$ over a broad range ($\sim$16 cm^{-1}), demonstrating the potential for simultaneously recording the complex spectra of multiple species. This capability allows the identification of a particular species of interest with high sensitivity and selectivity. The measured spectra are in excellent agreement with the spectra from the high-resolution transmission molecular absorption database [J. Quant. Spectrosc. Radiat. Transfer **96**, 139–204 (2005)]. We also conduct WMS for the first time using an external cavity quantum cascade laser, a technique that enhances the sensitivity of detection. By employing WMS, we could detect low-intensity absorption lines, which are not visible in the simple absorption spectra, and demonstrate a minimum detection limit at the 100 ppb level with a short-path absorption cell. Details of the tunable, external cavity quantum cascade laser system and its performance are discussed. © 2009 Optical Society of America

OCIS codes: 000.2170, 010.1120, 120.6200, 280.3420, 300.1030, 300.6340.

1. Introduction

The accurate and precise monitoring of trace gases has applications in a wide range of fields, including the detection of environmental pollutants, tracking of contaminants in closed environmental systems, medical diagnostics, defense, and homeland security. Real-time trace gas detection is particularly important in environmental science (e.g., in atmospheric physics/chemistry concerning air quality control, as well as for complying with Environmental Protection Agency [1] air quality regulations and safety monitoring). In these applications, the concentrations of pollutants typically range from several parts per million to the parts-per-trillion level and thus require techniques that are both highly sensitive and selective. Nitrogen oxides (NO$_x$) are some of the more

damaging of these pollutants and have multiple impacts on the environment and public health. They play important roles in the formation of photochemical smog, the formation of tropospheric ozone, and the formation of acid rain.

Laser-based techniques for monitoring environmental pollutants in the air have several advantages over chemical and other techniques, especially their ability to provide real-time monitoring capabilities and greater sensitivity. Until recently, the approaches have included (i) observing the visible and near-IR overtones of molecular transitions (which are much weaker than the fundamental mid-IR transitions) using room-temperature tunable diode lasers [2–5]; (ii) observing the strong mid-IR transitions using tunable lead–salt diode lasers (which require cryogenic cooling and are typically multimode) [6] or strong tunable molecular laser systems such as CO lasers (which require cryogenic cooling and provide only limited tuning around the molecular lines

and overtones) [7,8]. The advent of the quantum cascade laser in the mid-IR region covering the 4–24 μm range has provided an attractive source for investigating the spectroscopy of trace gases in the atmosphere and constructing portable gas sensors [9]. Using quantum cascade lasers (which can operate in a room-temperature environment using thermoelectric cooling), one can access the strong mid-IR fundamental rotational–vibrational transitions of molecular species [10], thus offering improved sensitivity over techniques based on detecting the overtones of these lines. By employing an external cavity arrangement, a quantum cascade laser offers a narrow linewidth ($\Delta\nu \sim 0.001\,\mathrm{cm}^{-1}$), highly stable and reproducible tunable CW output, and a wide continuous tuning range, all of which are essential for the study of complex spectra, as is the case in investigating trace gas components in the atmosphere [11].

The current work focuses on using a quantum cascade laser operating at room temperature to detect NO_2 with high sensitivity and selectivity. The project's aim is to ultimately develop a portable, self-contained device that may be used for high-precision, *in situ* atmospheric measurements. To this end, a short-path absorption cell was used with a multipass configuration, and wavelength modulation techniques were employed to enhance the sensitivity. In wavelength modulation spectroscopy (WMS) [12–15], the laser output is modulated at a frequency (f), and detection is done at higher harmonics of the frequency (e.g., $2f$) so that the excess laser noise, which varies as $1/f$, is reduced, thereby enhancing the signal-to-noise ratio. Specifically, the modulation frequencies are lower than the absorption linewidth.

2. Experimental Details

The quantum cascade laser source was purchased from Daylight Solutions (Model TLS-CW-MHF) and has a tuning range of 1625 to 1645 cm^{-1}. The external cavity is of Littrow configuration, which allows a wide range of mode-hop-free tuning, provides a narrow linewidth ($\sim 0.001\,\mathrm{cm}^{-1}$) and is thus well suited for spectroscopic measurements. Because of manufacturing issues with the antireflective coating on the laser chip, the mode-hop-free tuning range did not span the entire 20 cm^{-1} tuning range of the laser system, but rather it was limited to the region between 1629 and 1645 cm^{-1}. We were able to record a continuous NO_2 spectrum over this 16 cm^{-1} range without mode hops. Between 1625 and 1629 cm^{-1}, the laser tuned over short ranges (of the order of 1 cm^{-1}) before hopping to another mode. The continuity and linearity of the laser tuning were monitored using an etalon and the laser controller's display screen, as well as by comparing recorded spectra with line positions identified in the high-resolution transmission molecular absorption (HITRAN) database [16]. The laser power varies as a function of tuning, with a minimum output power of 5 mW at 1625 cm^{-1} and a maximum of 18 mW at 1645 cm^{-1}.

The output power at 1632.5 cm^{-1} (where we conducted our WMS) was 8 mW. Broad-range tuning is achieved entirely by rotating the external cavity grating via a stepper motor; no current or temperature tuning was necessary. The system may be set to one of six preset tuning rates, the slowest of which was 3.125 cm^{-1}/s (the tuning rate used to record our NO_2 absorption spectra). A piezoelectric transducer (PZT) positioned between the stepper motor and the grating itself allows one to tune smoothly at any desired rate over a smaller range (1 cm^{-1}) as well as modulate the laser frequency with a sinusoidal signal (allowing us to perform WMS). Additionally, its room-temperature operability and compact size make it a suitable candidate for a portable device for *in situ* measurements.

We carried out absorption spectroscopy of NO_2 using a short-path absorption cell (12.5 cm) filled with different concentrations of NO_2. The schematic of the experimental arrangement is shown in Fig. 1. Two rectangular, flat, protected gold mirrors were aligned to reflect the beam back and forth nine times through the cell, creating a homemade multipass cell that increased the path length to 1.125 m. The signal was detected using a two-stage, TE-cooled, IR photovoltaic detector (PVI-2TE-8 manufactured by Vigo), which can be operated in a room-temperature environment. The detectors were optically immersed in a high refractive index, hyperhemispherical lens. Phase-sensitive detection was done using a chopper running at 3.9 kHz and a lock-in amplifier (Stanford Research Systems SR830 DSP) with the time constant set to 3 ms.

The NO_2 mixtures used were prepared by loading the experimental cell with a precalibrated 1% mix of NO_2 and 99% N_2 (mixed and certified by National Specialty Gases to $\pm 2\%$ of the specified concentration) to a desired pressure. Additional pure N_2 was then added to increase the pressure to the desired final value. For example, for the 50 ppm concentration used for the absorption spectroscopy, the
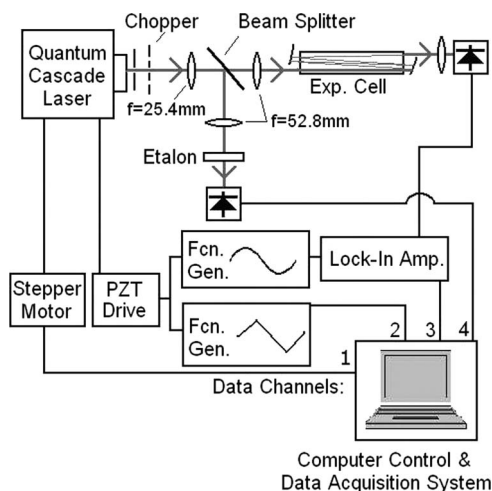

Fig. 1. Schematic of the experimental setup employed for absorption and WMS.

experimental cell was first loaded with $1.3 \pm 1\,\text{mbar}$ of the precalibrated 1% mix of NO_2 before additional pure N_2 was added to reach a final pressure of $260 \pm 20\,\text{mbar}$. Because of limitations in the accuracy of our vacuum/mixing apparatus, the mixed concentrations are expected to be accurate to $\pm 20\%$. The mixing apparatus was tested by generating several concentrations of NO_2 and comparing the recorded absorption line intensities with the calculated intensities based on HITRAN. This confirmed that the mixtures were within the expected uncertainty.

Experiments in the mid and far-IR typically suffer from significant etalon effects. We identified etaloning in our signal due to a beam splitter and the original cell windows. The etalon effects from the beam splitter were removed by placing it between the lenses of a 2× beam expander ($f_1 = 25.8\,\text{mm}$, $f_2 = 50.6\,\text{mm}$); the short focal lengths were necessary to create enough divergence to remove the etalon peaks. Wedge windows (Ar-coated ZnSe with faces that were 1° away from parallel) were used in the cell to remove its etaloning. The quantum cascade laser itself exhibited etaloning due to its antireflection coatings. We compensated for this by subtracting empty-cell scans of the laser (which characterized the laser's tuning characteristics, including etaloning) from scans of the cell loaded with NO_2.

Quantum cascade lasers are sensitive to optical feedback. As there are no faraday rotators currently available to construct an optical isolator to work with $6.1\,\mu\text{m}$ radiation, we aligned our apparatus to minimize the amount of radiation that was back-reflected to the laser. For example, the cell was oriented such that its windows were slightly offset from normal to the beam, and $1\,\text{mm}$ apertures were used to block any stray radiation from reflecting back into the laser.

We report WMS data conducted on NO_2 samples using the multipass geometry described earlier. The laser was tuned across the transitions of interest (via its PZT) using a slow triangle wave of $0.1\,\text{Hz}$. A higher-frequency sine wave ($130\,\text{Hz}$) was superimposed on this ramp to modulate the laser for WMS. The second harmonic signal was recorded at the modulation frequency $2f$ (the lock-in amplifier time constant used was $10\,\text{ms}$). The amplitude of the sine wave is specified via the modulation parameter m:

$$m = \frac{a}{\Delta \nu},$$

where $\Delta \nu$ is the half-width at half-maximum (HWHM) of the corresponding spectral line, and a is the modulation depth. To determine the HWHM, we needed to look closely at the transitions being studied. Our initial target was a strong, closely spaced doublet from the R band with an intensity $\sim 10^{-19}\,\text{cm/molecule}$ from the transitions between the (0 0 1)–(21 2 19) and (0 0 0)–(20 2 18) levels, and whose individual lines are located at 1632.508

and 1632.511 cm^{-1} (note that the $(\nu_1\,\nu_3\,\nu_3)$–$(N\,K_a\,K_c)$ level notation is used). The separation of the lines within this doublet is $0.003\,\text{cm}^{-1}$, which is much less than the pressure broadened widths of the lines at $120\,\text{mbar}$, meaning that it should show as a single absorption "line." We measured the HWHM of the resulting unresolved line to be $\sim 0.018\,\text{cm}^{-1}$ and used this value for purposes of determining the modulation depth of the sine wave. A modulation parameter of $m = 2.2$ HWHM was used (which corresponds to a sinusoidal tuning of $0.040\,\text{cm}^{-1}$). We studied several modulation depths and found the signal is maximum at $m = 2.2$, which agrees with the work of Reid and Lebrie [17]. The other transitions using WMS that are discussed in this paper were comprised of similarly closely spaced doublets, thus allowing us to use the same modulation depth.

The modulation frequency used was $130\,\text{Hz}$. Based on previous work in our lab using diode lasers for WMS of Rb, we would expect frequencies of the order of $1\,\text{kHz}$ or higher to provide stronger signals. However, the current external cavity design limits the modulation of the quantum cascade laser to much lower frequencies. Specifically, the mass of the grating assembly was too large for the PZT to modulate precisely at frequencies above $130\,\text{Hz}$. Attempts at higher frequencies resulted in a decrease in the signal-to-noise ratio and nonsinusoidal response of the system. The laser is to be upgraded in the near future to allow for higher modulation frequencies.

3. Results and Discussion

A. Absorption Spectroscopy

One of the most valuable aspects of the external cavity, tunable CW quantum cascade laser is its ability to tune over broad ranges without mode hops. To the best of our knowledge, we have recorded the first wide-range, continuous absorption spectra of NO_2 using a quantum cascade laser. The plot (Fig. 2) shows the spectra recorded from $1629\,\text{cm}^{-1}$ through to the end of the laser's tuning range at $1645\,\text{cm}^{-1}$.
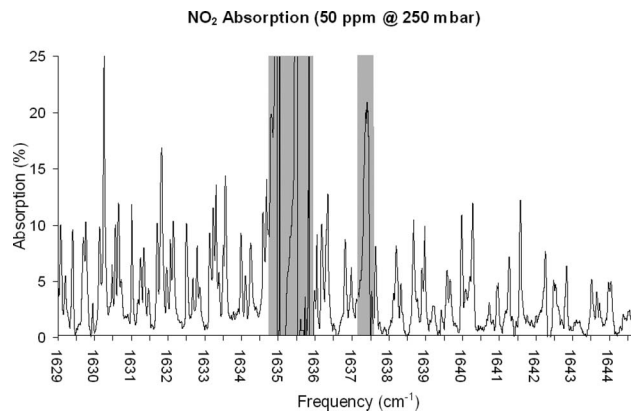

Fig. 2. NO_2 absorption spectrum recorded from 1629 to 1645 cm^{-1} at 50 ppm at 260 mbar, using a continuously tunable, external cavity quantum cascade laser.

This spectrum was recorded by loading the cell with NO_2 at 50 ± 10 ppm at a pressure of 260 ± 20 mbar, scanning the laser across the region, and then subtracting that trace from an empty-cell trace (the cell was evacuated to 2×10^{-4} mbar). The result was then divided by the empty-cell trace to compensate for variation in the laser power with tuning. Note that two strong water lines at 1634.97 and 1635.65 cm^{-1} masked NO_2 lines between 1634.7 and 1636 cm^{-1} (the water lines are from the transition between the (0 1 0)–(1 1 1) and (0 0 0)–(0 0 0) levels and the transition between (0 1 0)–(3 1 2) and (0 0 0)–(3 0 3) levels, respectively). Similarly, the moderately strong water line at 1637.51 cm^{-1} (from the transition between the (0 1 0)–(3 1 2) and (0 0 0)–(2 2 1) levels) masked the NO_2 lines between 1637.2 and 1637.5 cm^{-1}. In these regions (shaded in gray) the ambient water vapor in the beam path leading to the experimental cell completely or nearly completely absorbs the quantum cascade laser beam and overwhelms any NO_2 in that region. The apparent noise in the recorded spectrum results from our inability to completely subtract off the NO_2 trace from the empty-cell trace due to the saturation effects.

The recorded spectra were compared with simulated spectra generated using the HITRAN database and the SPECTRA software developed by Mikhailenko et al. [18]. We generated the spectrum with Voigt line shapes for the specifics of our experimental arrangement (50 ppm concentration at 260 mbar with a total path length of 1.125 m). Figure 3 shows the absorption and simulated spectra from 1631.74 to 1634.8 cm^{-1}, where a smaller range was used to facilitate their comparison. This spectrum shows 14 absorption features that result from approximately 200 NO_2 lines. However, a review of the HITRAN database shows that the observed structure of this absorption spectrum is primarily determined by 17 strong, closely spaced NO_2 doublets; the spacing of the lines within the doublets is ≤ 0.01 cm^{-1}, which is much less than their line width (FWHM

~ 0.07 cm^{-1} at 260 mbar). The remaining NO_2 lines in this region are one to four orders of magnitude weaker and do not make significant contributions to the observed features. Table 1 identifies the doublets and the corresponding absorption features in Fig. 3. The agreement between the experimental spectra and the spectra generated from the HITRAN database demonstrates the reliability of the external cavity quantum cascade laser for recording continuous spectra over a wide range of frequency.

B. Wavelength Modulation Spectroscopy

WMS was conducted on NO_2 at a concentration of 75 ± 15 ppm and a pressure of 120 ± 10 mbar using the same nine-pass absorption cell and beam expander detailed earlier. The lower pressure was chosen for the present measurements so that the NO_2 lines would be narrower and thus (1) facilitate the analysis of the second harmonic signal and (2) allow us to resolve certain desired weaker lines, which are used to determine the detection sensitivity. The WMS data were recorded using a slow scan of 0.1 Hz and sinusoidal modulation of 130 Hz.

Figure 4 shows the absorption spectrum of the doublet located at 1632.51 cm^{-1} corresponding to the transitions (0 0 1)–(21 2 19) and (0 0 0)–(20 2 18). The closeness of the doublet's spacing (0.003 cm^{-1}) results in what appears to be a single absorption line. The absorption feature that appears immediately to the right of the main peak, at 1632.54 cm^{-1}, is due to two closely spaced doublets that are approximately 10 and 15 times weaker than the main peak. This spectrum was recorded using a chopper at 3.9 kHz and lock-in detection (time constant = 10 ms). In this case, the laser was scanned using the PZT drive at 0.1 cm^{-1}/s instead of the stepper motor. The peak absorption is 13.6%, and the noise is approximately
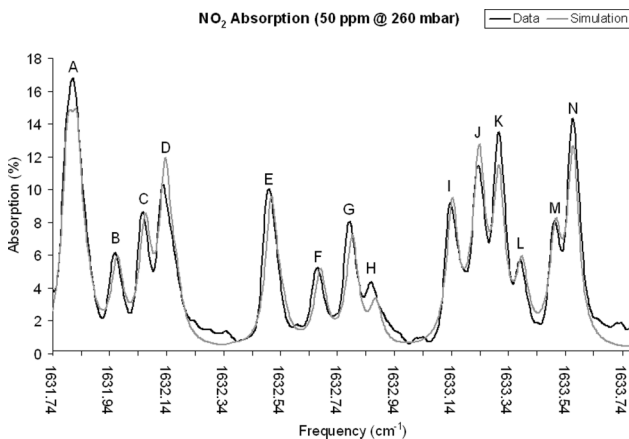

Fig. 3. Absorption spectrum of NO_2 (50 ppm at 260 mbar) from 1631.73 to 1633.8 cm^{-1} (the black trace is from the experimental data, and the gray trace is the simulated spectrum based on HITRAN data).

Table 1. Spectral Line Parameters from HITRAN for Major NO_2 Doublets in the *R* Branch Contributing to the Absorption Spectra Shown in Fig. 3

| Figure 3 Absorption Feature	Central Frequency of Doublet (cm^{-1})	Upper State $(\nu_1\,\nu_3\,\nu_3)-$ (N′K′$_a$K′$_c$))	Lower State $(\nu_1\,\nu_3\,\nu_3)-$ (N″K″$_a$K″$_c$)
A	1631.797	(0 0 1)-(19 0 19)	(0 0 0)-(18 0 18)
A	1631.828	(0 0 1)-(19 1 18)	(0 0 0)-(18 1 17)
B	1631.970	(0 0 1)-(24 4 21)	(0 0 0)-(23 4 20)
C	1632.068	(0 0 1)-(22 3 20)	(0 0 0)-(21 3 19)
D	1632.139	(0 0 1)-(20 1 20)	(0 0 0)-(19 1 19)
D	1632.175	(0 0 1)-(27 5 22)	(0 0 0)-(26 5 21)
E	1632.509	(0 0 1)-(21 2 19)	(0 0 0)-(20 2 18)
F	1632.683	(0 0 1)-(25 4 21)	(0 0 0)-(24 4 20)
G	1632.794	(0 0 1)-(23 3 20)	(0 0 0)-(22 3 19)
H	1632.876	(0 0 1)-(28 5 24)	(0 0 0)-(27 5 23)
I	1633.145	(0 0 1)-(22 2 21)	(0 0 0)-(21 2 20)
J	1633.240	(0 0 1)-(21 0 21)	(0 0 0)-(20 0 20)
K	1633.308	(0 0 1)-(21 1 20)	(0 0 0)-(20 1 19)
L	1633.389	(0 0 1)-(26 4 23)	(0 0 0)-(25 4 22)
M	1633.506	(0 0 1)-(24 3 22)	(0 0 0)-(23 3 21)
N	1633.568	(0 0 1)-(22 1 22)	(0 0 1)-(21 1 21)
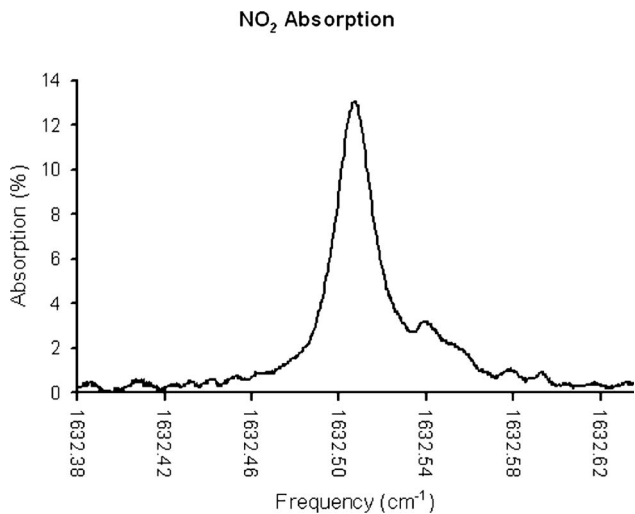
NO₂ Absorption

Fig. 4. NO₂ absorption spectrum of the doublet at $1632.5\,\mathrm{cm^{-1}}$. The NO₂ concentration was at $75 \pm 15\,\mathrm{ppm}$ at a pressure of $120 \pm 10\,\mathrm{mbar}$. The closely spaced doublet (1632.508 and $1632.511\,\mathrm{cm^{-1}}$) appears as one absorption feature. The weak absorption feature to the right of the main peak is from two closely spaced doublets that are approximately 10 and 15 times weaker than the main peak and are located at 1632.541 and $1632.544\,\mathrm{cm^{-1}}$.

0.3% of the absorption, resulting in a signal-to-noise ratio ∼50.

The second harmonic WMS signal of the NO₂ doublet at $1632.51\,\mathrm{cm^{-1}}$ presented in Fig. 5 shows that, as expected, the closely spaced doublet results in a single second harmonic signal. The second harmonic WMS signal from two closely spaced doublets at $1632.54\,\mathrm{cm^{-1}}$ is weaker and overlaps the high-frequency wing from the NO₂ doublet at $1632.51\,\mathrm{cm^{-1}}$.

To quantify the improvement in the signal-to-noise ratio and thus to determine the sensitivity of detection, we chose to analyze a weaker multiplet that is not clearly resolved in the absorption spectrum but
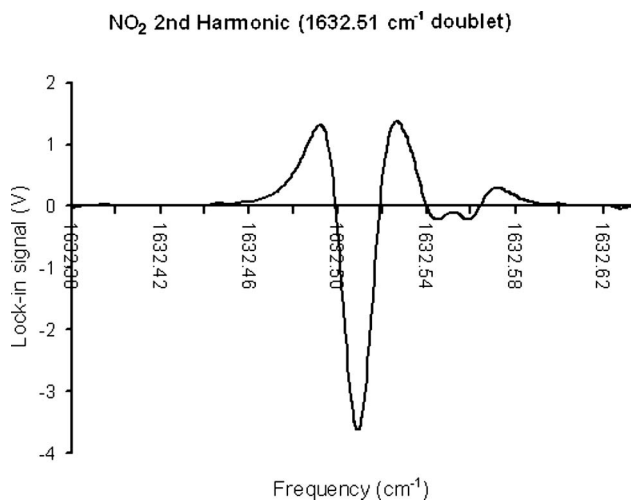
NO₂ 2nd Harmonic (1632.51 cm⁻¹ doublet)

Fig. 5. Second harmonic WMS signal of absorption spectrum of the doublet at $1632.5\,\mathrm{cm^{-1}}$. The NO₂ concentration was $75 \pm 15\,\mathrm{ppm}$ at a pressure of $120 \pm 10\,\mathrm{mbar}$.

can be seen in the second harmonic WMS spectrum [Fig. 6(a)]. This multiplet, centered at approximately $1632.385\,\mathrm{cm^{-1}}$, is comprised of two closely spaced doublets. The lines in the first of these two doublets are located at 1632.372 and $1632.375\,\mathrm{cm^{-1}}$, respectively, and result from the transitions between (0 1 1)–(37 0 37) and (0 1 0)–(36 0 36). They are separated by $0.003\,\mathrm{cm^{-1}}$ and at 120 mbar would not be resolved since the expected HWHM of a single line is $0.18\,\mathrm{cm^{-1}}$. Their intensities are 8.55×10^{-22} and $8.32 \times 10^{-22}\,\mathrm{cm/molecule}$, and the expected combined peak is approximately 120 times weaker than the strong doublet at $1632.509\,\mathrm{cm^{-1}}$ seen in Fig. 5. The lines in the second of these doublets are located at 1632.398 and $1632.403\,\mathrm{cm^{-1}}$, respectively, and result from the transitions between (0 1 1)–(38 2 37) and (0 1 0)–(37 2 36). They are separated by $0.005\,\mathrm{cm^{-1}}$ and would not be resolved. Their intensities are 6.36×10^{-22} and $6.19 \times 10^{-22}\,\mathrm{cm/molecule}$, and the expected combined peak is about 160 times weaker than the strong doublet at $1632.509\,\mathrm{cm^{-1}}$ seen in Fig. 5. The separation between the doublets themselves is ∼$0.037\,\mathrm{cm^{-1}}$, which is approximately
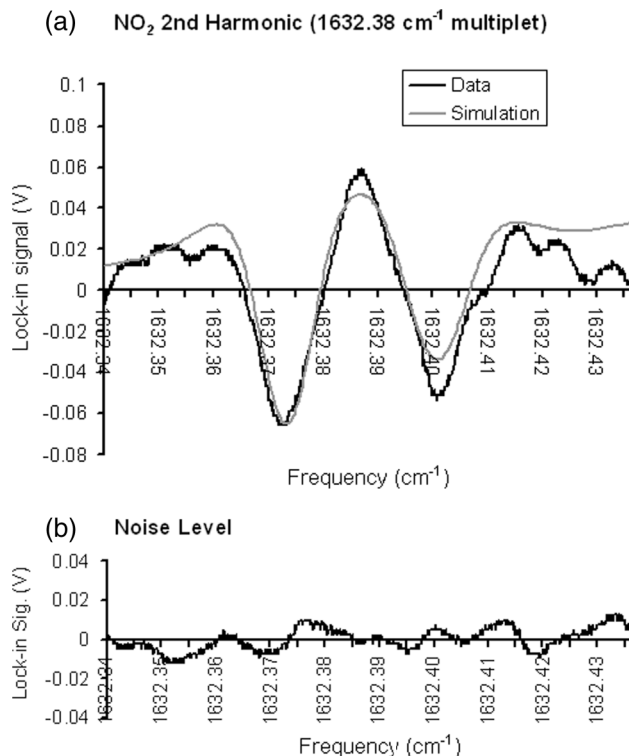
(a) NO₂ 2nd Harmonic (1632.38 cm⁻¹ multiplet)

(b) Noise Level

Fig. 6. (a) Second harmonic signal of the NO₂ multiplet at $1632.38\,\mathrm{cm^{-1}}$. The NO₂ concentration was $75 \pm 15\,\mathrm{ppm}$ at a pressure of $120 \pm 10\,\mathrm{mbar}$. The two doublets that comprise this feature are seen to partially overlap, as is expected. The black trace is from the experimental data, and the gray trace is the simulated spectrum based on HITRAN data. The agreement between the simulated spectrum and experimental data confirm that the two doublets are resolved as expected (the simulated spectrum was generated by exporting the table generated by the SPECTRA software and plotting its second derivative). (b) Noise content is shown for the same region and was obtained under the same operating conditions but with an empty cell.

the FWHM of an individual line, and is resolved in Fig. 6(a). It should be noted that each of the negative peaks of the second harmonic WMS signal in Fig. 6(a) are located at the position of the corresponding doublet's absorption peak. The positive peak at $1632.385\,\mathrm{cm}^{-1}$ in Fig. 6(a) is due to the additive overlap in the second harmonic WMS signal from the two doublets. Specifically, it is from the high-frequency wing of the $1632.37\,\mathrm{cm}^{-1}$ doublet and the low-frequency wing of the $1632.40\,\mathrm{cm}^{-1}$ doublet. As a result, the amplitude of the signal in Fig. 6(a) corresponds to a transition that is approximately 100 times weaker than the strong $1632.51\,\mathrm{cm}^{-1}$ doublet in Fig. 5. We compare the amplitude of the signal (peak-to-peak lock-in voltage $= 0.12\,\mathrm{V}$) to the noise spectrum seen in Fig. 6(b) (which was obtained under the same operating conditions but with an empty cell). The noise spectrum has a peak-to-peak lock-in voltage of $0.02\,\mathrm{V}$, which means that the signal-to-noise ratio for the multiplet in Fig. 6(a) is approximately 6. Based on the NO_2 concentration of 75 ppm, the relative strengths of the strong $1632.51\,\mathrm{cm}^{-1}$ doublet and the weaker $1632.385\,\mathrm{cm}^{-1}$ multiplet, and the signal-to-noise ratio, we report that the apparatus is capable of detecting NO_2 concentrations at the 100 ppb level.

4. Conclusion

We report for the first time absorption and WMS of NO_2 using an external cavity, tunable CW quantum cascade laser. In particular, the use of an external cavity quantum cascade laser enabled us to record continuous, mode-hop-free spectra over a $16\,\mathrm{cm}^{-1}$ range. The capability to tune over a wide range would be very useful in recording and interpreting the complex spectra normally observed with atmospheric trace gas detection. We also demonstrated WMS of NO_2, a technique that enhances the sensitivity of detection. Employing WMS with a short-path absorption cell, we report the sensitivity of detection of NO_2 at the 100 ppb level. We conclude that a tunable, external cavity quantum cascade laser provides a significant advantage over other laser sources for the detection of multiple gas species in the environment with high sensitivity and specificity.

References

1. "National air quality, monitoring and emissions trends report," EPA Report 450/2-78-052, United States Environmental Protection Agency, Washington DC, 1978.
2. L. Gianfrani, G. Gagliardi, G. Pesce, and A. Sasso, "High-sensitivity detection of NO_2 using a 740 nm semiconductor diode laser," Appl. Phys. B **64**, 487–491 (1997).
3. A. Schmol, A. Miklós, and P. Hess, "Detection of ammonia by photoacoustic spectroscopy with semiconductor lasers," Appl. Opt. **41**, 1815–1823 (2002).
4. D. B. Oh and A. C. Stanton, "Measurement of nitric oxide with an antimonide diode laser," Appl. Opt. **36**, 3294–3297 (1997).
5. J. Wang, M. Maiorov, D. S. Baer, D. Z. Garbuzov, J. C. Connolly, and R. K. Hanson, "*In situ* combustion measurements of CO with diode laser absorption near $2.3\,\mu\mathrm{m}$," Appl. Opt. **39**, 5579–5589 (2000).
6. P. Werle, "Analytical applications of infrared semiconductor lasers in atmospheric trace gas monitoring," J. Phys. IV **4**, C4-9–C4-12 (1994).
7. M. Mürtz, B. Frech, P. Palm, R. Lotze, and W. Urban, "Tunable carbon monoxide overtone laser sideband system for precision spectroscopy from 2.6 to $4.1\,\mu\mathrm{m}$," Opt. Lett. **23**, 58–60 (1998).
8. F. G. C. Bijnen, F. J. M. Harren, J. H. P. Hackenstein, and J. Reuss, "Intracavity CO laser photoacoustic trace gas detection: cyclic CH_4, H_2O and CO_2 emission by cockroaches and scarab beetles," Appl. Opt. **35**, 5357–5368 (1996).
9. A. A. Kosterev, R. F. Curl, F. K. Tittel, M. Rochat, M. Beck, D. Hofstetter, and J. Faist, "Chemical sensing with pulsed QC–DFB lasers operating at $15.6\,\mu\mathrm{m}$," Appl. Phys. B **75**, 351–357 (2002).
10. F. K. Tittel, Y. Bakhirkin, A. Kosterev, and G. Wysocki, "Recent advances in trace gas detection using quantum and interband cascade lasers," Rev. Laser Eng. **34**, 275–282 (2006).
11. G. Wysocki, R. Curl, F. Tittel, R. Maulini, J. Billiard, and J. Faist, "Widely tunable mode-hop free external cavity quantum cascade laser for high resolution spectroscopic applications," Appl. Phys. B **81**, 769–777 (2005).
12. R. Arndt, "Analytical line shapes for Lorentzian signals broadened by modulation," J. Appl. Phys. **36**, 2522–2524 (1965).
13. A. N. Dharamsi, "A theory of modulation spectroscopy with applications of higher harmonic detection," J. Phys. D **29**, 540–549 (1996).
14. L. C. Philippe and R. K. Hanson, "Laser diode wavelength-modulation spectroscopy for simultaneous measurement of temperature, pressure, and velocity in shock-heated oxygen flows," Appl. Opt. **32**, 6090–6103 (1993).
15. H. Li, G. B. Rieker, X. Liu, J. B. Jeffries, and R. K. Hanson, "Extension of wavelength modulation depth for diode laser absorption measurements in high-pressure gases," Appl. Opt. **45**, 1052–1061 (2006).
16. L. S. Rothman, D. Jacquemart, A. Barbe, D. C. Benner, M. Birk, L. R. Brown, M. R. Carleer, C. Chackerian, Jr., K. Chance, L. H. Coudert, V. Dana, V. M. Devi, J.-M. Flaud, R. R. Gamache, A. Goldman, J.-M. Hartmann, K. W. Jucks, A. G. Maki, J.-Y. Mandin, S. T. Massie, J. Orphal, A. Perrin, C. P. Rinsland, M. A. H. Smith, J. Tennyson, R. N. Tolchenov, R. A. Toth, J. Vander Auwera, P. Varanasi, and G. Wagner, "The HITRAN 2004 molecular spectroscopic database," J. Quant. Spectrosc. Radiat. Transfer **96**, 139–204 (2005).
17. J. Reid and D. Labrie, "Second-harmonic detection with tunable diode lasers—comparison of experiment and theory," Appl. Phys. B **26**, 203–210 (1981).
18. C. N. Mikhailenko, Yu. L. Babikov, and V. F. Golovko, "Information-calculating system spectroscopy of atmospheric gases. The structure and main functions," Atmos. Oceanic Opt. **18**, 685–695 (2005).